Numerical Investigation of the Dynamics of a Thin Film Type II Superconductor with and without Disorder

A.K.Kienappel and M.A.Moore
Department of Physics, University of Manchester, Manchester, M13 9PL, United Kingdom.
(February 1, 2008)

The equilibrium dynamics of a thin film type II superconductor with spherical geometry are investigated numerically in a simulation based on the lowest Landau level approximation to the time-dependent Ginzburg-Landau equation. Both the static and time-dependent density-density correlation functions of the superconducting order parameter have been investigated for systems with varying amounts of quenched random disorder. As the temperature is lowered it is found that the correlation length, the length-scale over which the vortices have short-range crystalline order, increases but the introduction of quenched random disorder reduces this correlation length. We see no signs of a phase transition in either the pure or the disordered case. For the disordered system there is no evidence for the existence of a Bragg glass phase with quasi long-range correlations. The dynamics in both the pure and disordered systems is activated, and the barrier of the relaxation mechanism grows linearly with the correlation length. The self-diffusion time scale of the vortices was also measured and has the same temperature dependence as that of the longest time scales found in the time dependent density-density correlation function. The dominant relaxation mechanism observed is a change in orientation of a correlated region of size of the correlation length. A scaling argument is given to explain the value of the barrier exponent.

PACS numbers: 74.20.De, 74.60.Ge, 74.76.-w

I. INTRODUCTION

The nature of the mixed state of thin films of type II superconductors is despite considerable experimental, theoretical and numerical research still unclear. In the mean-field limit, which describes the ground state of the system, the vortices are known to form into a triangular Abrikosov lattice [1]. Also it is generally accepted that close to the mean-field transition line to the normal state, the H_{c2} line, thermal fluctuations destroy that hexagonal order and lead to a vortex liquid state [2]. However, the phase diagram between the mean-field H_{c1} and H_{c2} lines remains unclear. The Kosterlitz-Thouless-Halperin-Nelson (KTHN) theory of a two dimensional (2D) melting [3] has been applied to superconductors [4] [5] yielding a phase diagram with a solid, a hexatic and a liquid phase. Other theoretical work raises a doubt as to whether there is *any* phase transition to the mixed state and suggests that a flux lattice exists only in the zero temperature limit and that the liquid phase exists at any non-zero temperature [6] [7]. It has long been predicted that in the presence of disorder any long range crystalline order of a vortex lattice phase is destroyed in less than four dimensions [8]. In the glass like state which is expected to form instead, the length scale of the short-range crystalline order has been predicted by Ovchinnikov and Larkin [9] for the zero-temperature (mean-field) limit. More recently the existence of a Bragg glass phase with quasi long range order has been suggested [10]. The non-perturbative analytical method used by Yeo and Moore [7], which yields a 2D flux liquid at all temperatures, has also been applied to the case of quenched random disorder, which is found to just reduce the extent of short-range crystalline order present in the liquid state. We shall find good agreement of our numerical results with this work, but none with the KTHN picture, or in the presence of disorder with the Bragg glass scenario.

A lot of numerical work has been done on clean systems, some indicating a first order 2D vortex melting transition [11] [12] and some failing to see any kind of phase transition [13] [14] [15]. The experimental evidence on superconducting films is also contradictory. Whilst a first order 2D melting transition has never been observed, current-voltage measurements have provided some evidence for second order 2D melting [16] as well as failing to provide evidence for any transition in other experiments [17]. Yazdani et al. [18] have reported evidence for 2D melting from measurements of ac penetration depth in thin films of α- MoGe. Theunissen et al. [19] find indication of a melting as well as a hexatic to liquid transition in measurements of vortex viscosity in NbGe.

Most of this experimental evidence is on transport phenomena in samples that have at least weak disorder or surface pinning due to crystal defects or impurities. This focuses interest on the dynamics of the mixed state and the influence of quenched random disorder. For the description of ac transport phenomena equilibrium dynamics is relevant. It is also vital for the whole picture of the mixed state. It has been suggested that the apparent second order freezing transition deduced from changes in vortex liquid viscosity or sample resistance may instead be due to an exponentially fast increase of the relaxation time scales at low temperatures. [20]. This behavior, which our work confirms, indicates activated

dynamics, in which the relaxational time scales increase exponentially with the correlation length.

In this paper we present a numerical investigation into relaxational time scales of density correlations in the vortex liquid and diffusion time scales of the vortices in a thin film. A Langevin dynamics simulation is used with a phenomenological Ginzburg-Landau Hamiltonian. To simulate quenched random disorder, we add a Gaussianly-distributed random contribution to the mean-field transition temperature in the Hamiltonian. The equilibrium dynamics of the superconductor is investigated by measurements of the time scales of density correlation decay and vortex self-diffusion. We find that the time scales of the two different processes both show the same exponential growth with the translational correlation length in the system and are due to the same activated relaxation process.

The paper is organized as follows. In Section II we shall give a short summary of the background of the phenomenological Ginzburg-Landau theory on which our work is based. We then give a description of how we solve the time dependent Ginzburg-Landau equation numerically in Section III. Section IV reports our work on the density correlations and their relaxation times, followed by Section V which reports on self-diffusion of the vortices. In Section VI we put together our results from the previous sections and interpret them. We also identify the underlying dynamic processes. In Section VII we summarize and discuss our results.

II. THEORETICAL FRAMEWORK

Our simulation is based on the phenomenological Ginzburg-Landau theory in the approximation of a uniform magnetic field $\mathbf{B}$. The free energy functional for a clean sample is given by

$$F = \int d^3r \left(\alpha|\psi|^2 + \frac{\beta}{2}|\psi|^4 + \frac{1}{2m}|(-i\hbar\nabla - 2e\mathbf{A})\psi|^2 \right), \tag{1}$$

where ψ is the order parameter representing the macroscopic wave function of the superconducting electrons and $\mathbf{B} = \nabla \times \mathbf{A}$. In first approximation $\alpha(T) = \alpha'(T - T_c)$ and $\beta(T)$ is a constant. $\alpha', \beta > 0$.

For the case of quenched disorder a random local potential is added to the free energy:

$$F_{dis} = \int d^3r\, \Theta(\mathbf{r})|\psi(\mathbf{r})|^2, \tag{2}$$

where $\Theta(\mathbf{r})$ is real and Gaussian distributed with

$$\langle \Theta(\mathbf{r}) \rangle = 0, \tag{3}$$

$$\langle \Theta(\mathbf{r})\Theta(\mathbf{r}') \rangle = \Delta\delta(\mathbf{r} - \mathbf{r}'). \tag{4}$$

Angular brackets denote thermal averages and δ is the three dimensional Dirac delta function. Δ is the measure of the strength of the disorder.

The simulation follows Langevin dynamics, described by the time dependent Ginzburg-Landau equation.

$$\frac{\partial\psi(\mathbf{r},t)}{\partial t} = -\Gamma\, \frac{\partial F}{\partial \psi^*} + \xi(\mathbf{r},t), \tag{5}$$

where F is defined in Eq. (1) and ξ is Gaussian white noise of strength $2\Gamma k_B T$, i.e.

$$\langle \xi^*(\mathbf{r},t)\, \xi(\mathbf{r}',t') \rangle = 2\Gamma\, k_B T\, \delta(\mathbf{r} - \mathbf{r}')\delta(t - t') \; .$$

III. NUMERICAL SOLUTION OF THE TIME DEPENDENT GINZBURG-LANDAU EQUATION

We base our simulation on a thin film superconductor with the following experimentally realizable two dimensional geometry. A thin film superconducting sphere of radius R and thickness d is placed in a radial magnetic field of magnitude B which emerges from an infinitely long, thin solenoid whose end is at the center of the sphere. This system has been investigated numerically before, using Monte Carlo dynamics [13] [14] [15]. The reasons for our preference of this geometry to the more widely used geometry of a plane with periodic boundary conditions have been presented in detail by Dodgson and Moore [15]. The main advantage is that the spherical geometry guarantees full translational symmetry, which periodic boundary conditions do not, while having the same thermodynamic limit. Periodic boundary conditions impose an artificial pinning potential on the vortices which makes them unsuitable for investigating transport and dynamical phenomena.

We assume that in a strong type II superconductor where the magnetic penetration depth is larger than the coherence length of the superconducting wave function by orders of magnitude, fluctuations in the magnetic induction are negligible. Flux quantization requires that the B field at the sphere be such that $4\pi R^2 B = N\Phi_0$, where $\Phi_0 = h/2e$ is the flux quantum and N is the number of vortices. This fixes $R = \sqrt{N/2}$ with the unit of length being $l_m = \sqrt{\Phi_0/2\pi B}$, which is proportional to the nearest neighbor distance of vortices in the Abrikosov lattice.

We shall make the usual approximation of retaining only the lowest Landau level (LLL). This is the approximation that Abrikosov used to first describe the vortex lattice state at mean-field level [1]. Defining $\mathbf{D}$ as the gauge invariant momentum operator, $\mathbf{D} = -i\hbar\nabla - 2e\mathbf{A}$, the LLL is the eigenspace of D^2 associated with its lowest eigenvalue $2eB\hbar$. The LLL approximation is traditionally believed to hold near the upper critical field H_{c2}.

However, due to renormalization effects, it actually describes a large portion of the vortex liquid regime [21].

In spherical geometry an orthonormal basis of the LLL is [22]

$$\psi_m(\theta,\phi) = (4\pi R^2)^{-1/2} A_m e^{im\phi} \sin^m(\theta/2)\cos^{N-m}(\theta/2), \tag{6}$$

where N is the number of vortices, $0 \le m \le N$, and $A_m = B(m+1, N-m+1)^{-1/2}$. B stands for the Beta function, given for natural numbers n,m by

$$B(n,m) = \frac{(n-1)!\,(m-1)!}{(n+m-1)!}.$$

The order parameter in the LLL approximation can be expanded in the above basis set:

$$\psi(\theta,\phi) = Q \sum_{m=0}^{N} v_m \psi_m(\theta,\phi), \tag{7}$$

where $Q = (\Phi_0 k_B T/\beta d B)^{1/4}$ [15].

The free energy Hamiltonian for our system is given as a sum of the Hamiltonian of the clean system and the contribution from disorder, $\mathcal{H} = \mathcal{H}_{cl} + \mathcal{H}_{dis}$, where $\mathcal{H}_{cl}$ and $\mathcal{H}_{dis}$ are the free energy terms from Eqs. (1) and (2) respectively. If the order parameter is now expanded in the LLL eigenstates, we can carry out the spatial integral to express the Hamiltonian of a system without disorder in terms of the LLL coefficients v_m:

$$\frac{\mathcal{H}_{cl}(\{v_m\})}{k_B T} = \alpha_T \sum_{m=0}^{N} |v_m|^2 + \frac{1}{2N}\sum_{p=0}^{2N} |U_p|^2. \tag{8}$$

The effective temperature parameter is given by

$$\alpha_T = \frac{dQ^2}{k_B T}\left(\alpha(T) + \frac{eB\hbar}{m}\right). \tag{9}$$

Note that $\alpha_T = 0$ corresponds to the mean-field $H_{c2}(T)$ line and $\alpha_T = -\infty$ to $T = 0$. In the quartic term,

$$U_p = \sum_{q=0}^{N} \theta(p-q)\theta(N-(p-q))\, f_N(q,p-q)\, v_q v_{p-q}, \tag{10}$$

where θ is the Heaviside step function and

$$f_N(m,n) = (A_m A_n\, B(m+n+1,\, 2N-m-n+1))^{1/2}.$$

To express the disorder contribution $\mathcal{H}_{dis}$ in terms of the LLL coefficients v_m, we expand the random Gaussian disorder on the sphere in normalized spherical harmonics Y_l^m:

$$\Theta(\theta,\phi) = \frac{k_B T}{dQ^2}\sum_{l=0}^{\infty}\sum_{m=-l}^{l} a_l^m Y_l^m(\theta,\phi)$$

with $a_l^{m\,*} = a_l^{-m}$. To satisfy Eqs. (3) and (4), the real and imaginary parts of the a_l^m are drawn independently from a Gaussian distribution with variance $D = (dQ^2/k_B T)^2\Delta/2$ for $m \neq 0$ and the a_l^0 from a Gaussian with variance $2D$. Then the part of the Hamiltonian due to disorder can then be expressed

$$\frac{\mathcal{H}_{dis}(\{v_m\})}{k_B T} = \sum_{p,q=0}^{N}\sum_{l=|p-q|}^{N} a_{l,p-q} v_p^* v_q\; I^{|p-q|}_{l,(p+q-|p-q|)/2} \tag{11}$$

where

$$I_{l,n}^m = \int d^2 r Y_l^m \psi_{n+m}^* \psi_n \tag{12}$$

$$= A_n A_{n+m}\sqrt{\frac{(2l+1)(l+m)!}{4\pi(l-m)!}}\frac{(-1)^m}{m!}B(N-n+1,n+m+1) \times {}_3F_2\left(\begin{matrix} m-l,\, m+l+1,\, n+m+1, \\ m+1,\, N+m+2\,;\, 1\end{matrix}\right)$$

with ${}_3F_2$ a generalized hypergeometric function. This term of the Hamiltonian limits our simulation in the case of disorder to a relatively small system size, as it requires finding and storing $\sim N^3/6$ values of ${}_3F_2$. However, as the correlation length is very much reduced by disorder, the effects of the finite system size are for the same α_T much reduced compared with the non-disordered case.

The time dependent Ginzburg-Landau equation, discretized in time, which drives our simulation is now:

$$\begin{aligned} &v_m(t+\Delta t) - v_m(t) \\ &= -\Delta t\,\Gamma \frac{\partial(\mathcal{H}_{cl}(t) + \mathcal{H}_{dis}(t))}{\partial v_m^*} + \Delta t\,\xi_m(t) \end{aligned} \tag{13}$$

with $\mathcal{H}_{cl}(t)$ and $\mathcal{H}_{dis}(t)$ as defined in Eqs. (8) and (11).

This equation ensures that thermal averages can be replaced by time averages over successive measurements from the simulation. It leads to the correct canonical distribution after infinite time in the limit $\Delta t \to 0$ if real and imaginary parts of the ξ_m are drawn independently from a Gaussian probability distribution with variance $\sigma^2/\Delta t$ with $\sigma^2 = 2\,\Gamma\, k_B T$ [23]. However, the finite time steps always lead to a certain small deviation from the correct distribution, which does not arise in a Monte Carlo algorithm [24]. We have tested our simulation's static thermal averages for varying quantities like energy and entropy against Monte Carlo averages from the code used in Ref. [15], and chose our time steps $\Delta t = 0.15$, which reduces deviations to less than 1.5%.

The quenched disorder is self-averaging for the case of an infinite system. In a finite system though, the particular random choice of disorder will obviously influence the results. To reduce this effect we run the simulation between 10 and 20 times with different sets of random a_l^m, and average over these different measurements.

IV. THE DENSITY-DENSITY CORRELATOR

To investigate the extent of order and the time scales of fluctuations in the system, we compute the connected part of the density-density correlator. This correlator measures the correlations of the magnitude of the order parameter in space and time. The density-density correlator carries essentially the same information as the translational correlation function of the vortex positions [13]. However, it is far easier to compute than the latter, because it does not involve finding the zeros of the order parameter (see Section V). The density-density correlator is defined as

$$S(\mathbf{r}',t') = \langle|\psi(\mathbf{r},t)|^2|\psi(\mathbf{r}+\mathbf{r}',t+t')|^2\rangle - \langle|\psi(\mathbf{r},t)|^2\rangle\langle|\psi(\mathbf{r}+\mathbf{r}',t+t')|^2\rangle \quad (14)$$

This correlator and its decay in time is most revealing in $\mathbf{k}$ space if one is interested in the structure of the system. Therefore its Fourier transform is measured, normalized by the average density of the order parameter and for easier readability divided by its high temperature limit:

$$C(\mathbf{k},t) = \frac{S(\mathbf{k},t)}{\langle|\psi|^2\rangle^2} \times \lim_{\alpha_T\to\infty}\frac{\langle|\psi|^2\rangle^2}{S(\mathbf{k},0)} \quad (15)$$

To compute this quantity the concept of the Fourier transform on a plane has to be adapted to the curved two dimensional space of the surface of a sphere. The Fourier transform is an expansion of the correlation function in the complete orthonormal set of functions solving the free wave equation, which is in the plane the continuous set of functions $e^{i\mathbf{k}\cdot\mathbf{r}}$. The equivalent set of functions in a spherical geometry is the discrete set of normalized spherical harmonics, $Y_l^m(\mathbf{r})$. To a value of l corresponds $k = l/R$. Because the system is isotropic, the correlator in $\mathbf{k}$ space depends only on the magnitude of k, i.e. only on l and not on m. So, for better averaging we always calculate the correlator for all m and average over the different m.

$$S(l/R,t) = \frac{1}{2l+1}\sum_{m=-l}^{l}\int d^2r\, Y_l^m(\mathbf{r})S(\mathbf{r},t). \quad (16)$$

Now we substitute for $S(l/R,t)$ from Eq. (14), expand ψ in LLL eigenfunctions and take the spatial integral inside the thermal average and the summation over the lowest Landau levels. The high temperature limit can easily be worked out analytically [15] and the correlation function in Eq. 15 can be written in terms of thermal averages of the coefficients:

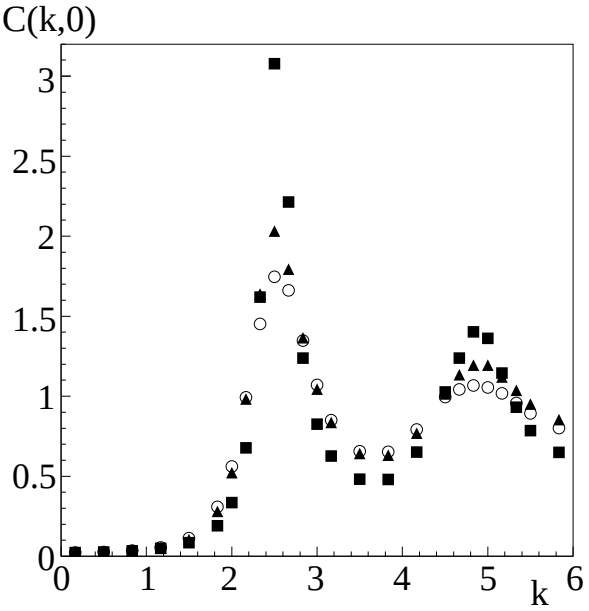

FIG. 1. Structure factor for $\alpha_T = -8$, squares represent D=0 (pure limit), triangles D=9, and circles D=25.

$$C(l/R,t-t') = \frac{4\pi(N-l)!(N+l+1)!}{(N!)^2(2l+1)}\frac{1}{\langle\sum_{n=0}^{N}v_n^*v_n\rangle} \times\sum_{m=-l}^{l}\left\langle\sum_{n=\max(0,-m)}^{\min(N,N-m)}v_{n+m}^*(t)v_n(t)I_{l,n}^m \times\sum_{n'=\max(0,-m)}^{\min(N,N-m)}v_{n'+m}^*(t')v_{n'}(t')I_{l,n}^m\right\rangle_c, \quad (17)$$

where $I_{l,n}^m$ is defined in Eq. 12. Here $\langle...\rangle_c$ signifies the connected part of the correlator, i.e. $\langle v_i^*(t)v_j^*(t')v_k(t)v_l(t')\rangle_c = \langle v_i^*(t)v_l(t')\rangle\langle v_j^*(t')v_k(t)\rangle$. Without disorder the non-connected part of the density-density correlator, denoted $C_{nc}(k,t)$, is zero for all $l\neq 0$, which is equivalent to translational invariance, $\langle|\psi(\mathbf{r},t)|^2\rangle$ constant. However, in the disordered case there are permanent correlations due to the structure imposed on the vortices by the quenched disorder. This is intuitively obvious: a permanent local potential will favor specific vortex constellations and thus result in permanent correlations. Therefore $\langle|\psi(\mathbf{r},t)|^2\rangle$ is a function of $\mathbf{r}$ and $C_{nc}(k,t)$ is not zero. The infinite time limit of the full correlator is equal to the non-connected part, for $t'\to\infty$ $\langle|\psi(\mathbf{r},t)|^2\psi(\mathbf{r}+\mathbf{r}',t+t')|^2\rangle = \langle|\psi(\mathbf{r},t)|^2\rangle\langle|\psi(\mathbf{r}',t')|^2\rangle$. We measure $C(k,t)+C_{nc}(k,t)$ directly. To retrieve the connected part, $C_{nc}(k,t)$ is subtracted.

A. The structure factor

The density-density correlator $C(k,t)$ for $t'=0$ is the structure factor of the system. For the case of no disorder it has been investigated in detail by Dodgson and

Moore [15]. We give a short summary of their results, which we will extend by adding disorder. The structure factor shows peaks (which sharpen as the temperature is lowered) near the inverse lattice vectors of the triangular vortex lattice. A Lorentzian always gives an excellent fit for the peak near the first reciprocal lattice vector. The associated correlation length ξ_D, (D for density), is proportional to the inverse width of this peak at half its maximum, (denoted by δ^{-1}), and found to vary as $\xi_D \propto |\alpha_T| l_m$.

Fig. 1 shows the structure factor at the same effective temperature for no, medium and very strong disorder. Disorder flattens the peaks of the structure factor and makes it look rather like that of a clean system at a higher temperature. Like for the clean case we can fit the first peak to a Lorentzian. However, the region around the peak where we get a good fit is narrower than in the clean case. Due to this limited fitting regime, the limited system size and, especially for strong disorder, insufficient averaging over disorder, the errors are rather large.

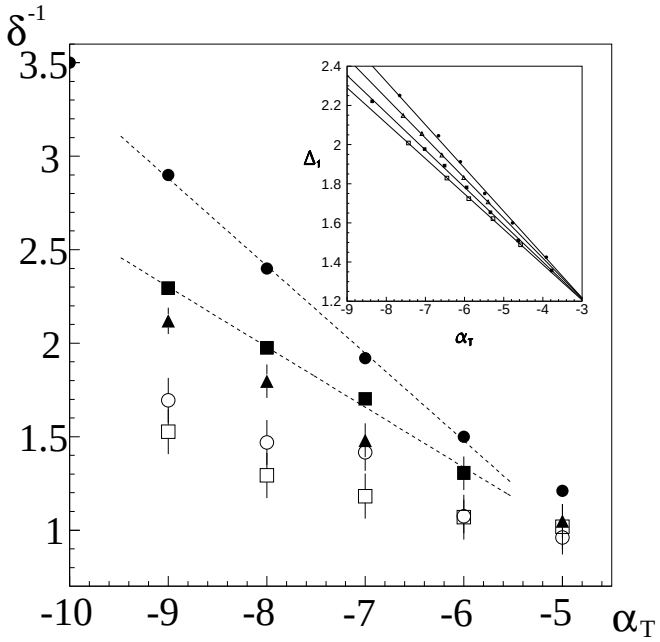

FIG. 2. The inverse width of the first peak in the structure factor depending on $-\alpha_T$ with linear fits to the region $-9 \leq \alpha_T \leq -6$. Filled circles, squares, triangles, empty circles and squares correspond to D=0 (pure limit), D=0.25, 1, 4 and 9 respectively. For D=0 the system size is N=200, for D≠0, N=72. The inset is reproduced from reference [7]. It shows equivalent results of the parquet graph approximation with linear fits for D=0, 0.1, 0.2 and 0.3.

Fig.2 shows the inverse peak width at half maximum, $\delta^{-1} \propto \xi_D$, from these fits for different degrees of disorder. At high temperatures the presence of disorder does not affect the correlation length ξ_D much. With decreasing temperature the growth of the correlation length is reduced. This effect is intuitively obvious because any hexagonal order is now opposed not only by thermal fluctuations but also by the pinning of vortices to randomly distributed potential minima. A linear growth of δ^{-1} with α_T and a decrease of the gradient $|\partial(\delta^{-1})/\partial\alpha_T|$ with increasing disorder has been predicted using a non-perturbative, parquet graph approximation to the two dimensional LLL system [7]. In the inset of Fig. 2 a plot of $\delta^{-1}(\alpha_T)$ from Ref. [7] is reproduced. We can now compare $\partial(\delta^{-1})/\partial\alpha_T$ from the parquet graph approximation with our simulation results. The absolute values of the gradients in the simulation are roughly a factor 2 larger than in Ref. [7]. However, the relative decrease of the gradient due to disorder agree well for Yeo and Moore's and our results. If we refer to the linear fits in Fig. 2 for the case of an increase of disorder from D=0 to D=0.5, the change in our simulation is only a factor 1.15 larger.

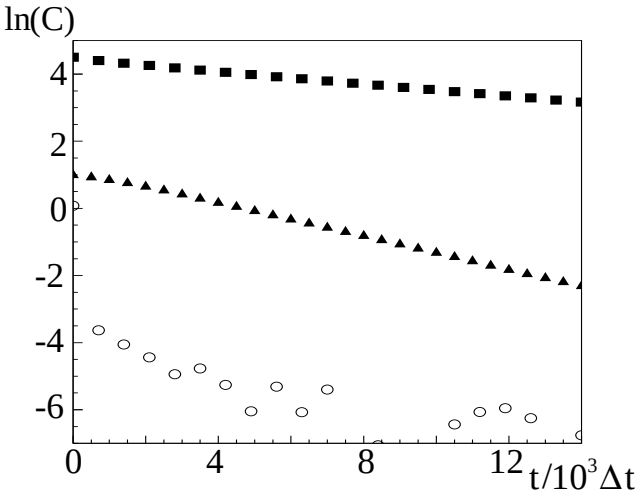

FIG. 3. Typical relaxation behavior for small k (k=0.5, circles) and for larger k (k=2.5) without disorder(squares) and with disorder (triangles)

B. Relaxation time scales

To discuss the relaxation time scales of the density-density correlator and their dependence on the wave vector, the effective temperature and the strength of disorder, we need to define a relaxation time $\tau_D(k, \alpha_T, D)$. Examples of the relaxation behavior of $C(k,t)$ with and without disorder are shown in Fig. 3. Without disorder $\ln(C(k,t))$ shows an almost perfectly linear decay with time. Only for very small times is the decay faster than in a linear fit. In the case of disorder however, the decay of $\ln(C(k,t))$ is linear only for later times and has a smaller gradient at earlier times. In this case we define τ_D from a fit only to the regime of truly linear exponential decay. We fit according to $C(k,t) \propto \exp(-t/\tau_D)$ to extract the relaxation time scale τ_D. This can be done

with great accuracy for larger k. However, with and without disorder, the error in this fit grows large for small k. For $k \leq 1.5$ we have $C(k,t) \ll 1$. The relaxation times are rather small in this regime and $C(k,t)$ decays very quickly to zero. Very near zero, however, noise dominates the data, so that in the worst cases we have to restrict our fits to the first two or three points of the curve.

Having defined τ_D from the exponential decay of the density-density correlator, it is an interesting observation that the time scales which arise from the exponential decay of the current correlator $\langle \nabla \times \mathbf{j}(\mathbf{r},t) \nabla \times \mathbf{j}(\mathbf{r}',t') \rangle$ which we measured when determining the transverse conductivity [25] are exactly the same. This suggests these time scales are important for all the dynamical properties of the system, as is bourne out by our results on the self-diffusion coefficient in Section V.

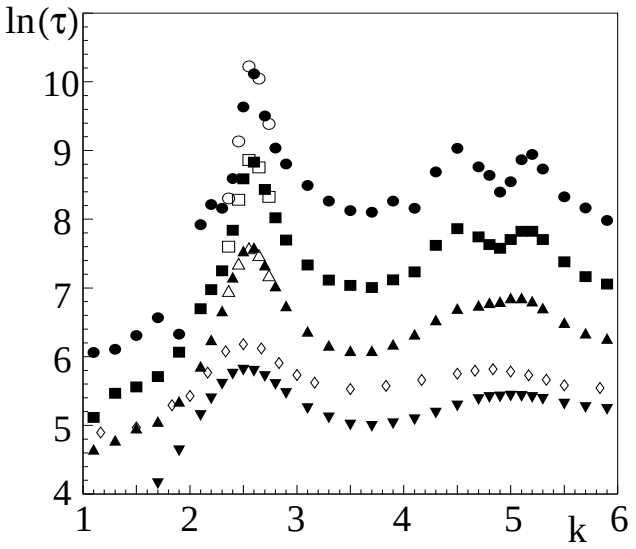

FIG. 4. Logarithmic Relaxation time scales of the decay of the density-density correlator in reciprocal space. Circles, squares, triangles pointing up and down represent D=0 (pure limit) and α_T = -12,-10,-8 and -5 respectively. For filled symbols system size N=200, for empty symbols N=224. Diamonds represent D=4, α_T =-8 and N=72.

We find that, in the vortex liquid regime which we are investigating, $\tau_D(k, \alpha_T, D)$ reflects, like the structure factor, the hexagonal lattice structure of the ground state. Fig. 4 shows a logarithmic plot of the k dependence of the relaxation times for different temperatures and degrees of disorder. Peaks can clearly be seen near the first, second and third reciprocal lattice vector of a triangular lattice in k space, which lie at k values of 2.694, 4.665 and 5.387 [13]. Note that for the clean system at $\alpha_T \leq -10$ the second and third peak are clearly resolved, which is not the case for the structure factor in the same temperature regime. For all measured temperatures, the longest relaxation time occurs at the first peak, i.e. $k \approx G = 2.694$. If we introduce disorder to the system, the peaks near the reciprocal lattice vectors flatten and, like the structure factor, the relaxation times look very similar to the ones in a clean sample at higher temperature. The error in τ_D increases with disorder for all values of k. Like in the case of the structure factor, this arises from insufficient averaging over disorder. The α_T dependence of the longest time time scales $\tau_D(k \approx G)$ can be seen in a logarithmic plot in Fig. 5 for different degrees of disorder. For the case without disorder the same quantity is also plotted in Fig. 7 over the whole temperature range for which measurements were taken.

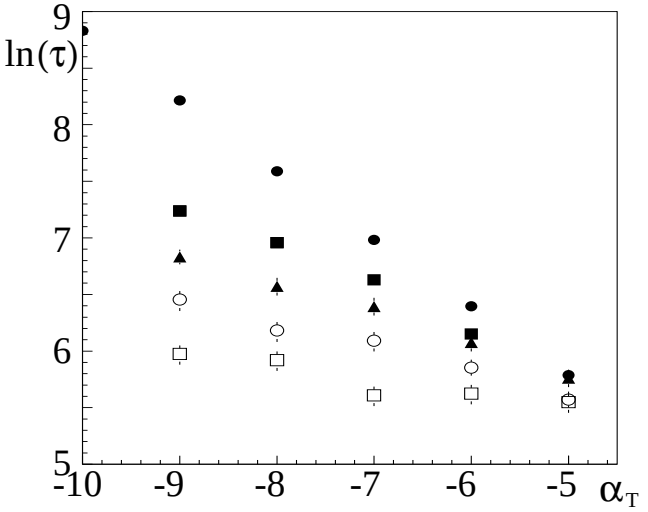

FIG. 5. Logarithm of the largest relaxation time scale versus $-\alpha_T$. Filled circles, filled squares, triangles, empty circles, and empty squares correspond to D=0, 0.25, 1, 4, and 9 respectively. For D=0 (pure limit) the system size is N=200, for D≠0, N=72.

Without disorder we see an almost perfectly linear exponential increase with $|\alpha_T|$, i.e. $\tau_D(G) \propto \exp(C|\alpha_T|)$. This indicates an activated relaxation process with an activation energy $E_a/k_BT \propto \ln(\tau_D) \propto |\alpha_T|$. With disorder a general decrease of the relaxation times can be observed. The effect of disorder is very small at high temperatures but grows stronger with decreasing α_T. With weak disorder the relation $\ln(\tau_D) \propto |\alpha_T|$ is, at least approximately, still valid, and for strong disorder holds also within the range of the increasingly large error. Further discussion of these results is left to Section VI.

V. SELF-DIFFUSION

We have measured the self-diffusion coefficient of the vortex positions **R**. In a liquid the square of the distance between initial position of a vortex and its position after time t, denoted by S(t), increases linearly in time because

of self-diffusion. The self-diffusion coefficient D_s is then defined from the following relation:

$$S(t) = \langle (\mathbf{R}(t) - \mathbf{R}(0))^2 \rangle = 2D_s\, t. \qquad (18)$$

In order to compute the self-diffusion coefficient we have to monitor the vortex positions on the sphere of over not too short a time interval. How the vortex positions depend on the LLL coefficients can easily be seen if we make a coordinate transformation in Eq. (7). We use the stereoscopic projection of the sphere into the complex plane, given by $z = x + iy = \cos(\phi)\tan(\theta/2) + i\sin(\phi)\tan(\theta/2)$. Now the order parameter expansion in Eq. (7) can be written as

$$\psi(z) = \frac{Q}{(2\pi N)^{1/2}(|z|^2+1)^N} \sum_{m=0}^{N} v_m A_m z^m. \qquad (19)$$

The vortices are where $\psi(z) = 0$, i.e. the roots of the Nth order polynomial with coefficients $v_m A_m$. For a typical system size of N=200, the 100th coefficient in these polynomials is about 60 orders of magnitude larger than the first and the last, which makes the numerical root finding nontrivial. With standard routines to find zeros of polynomials failing, we succeeded by searching for zeros on a very dense set of trial points using a Laguerre algorithm (see e.g. Ref. [26]). However, we cannot always find all vortices on the sphere. Vortices very close to the south pole, which is projected to infinity by the stereoscopic projection, can be inaccessible for the numerical routine. The number of these inaccessible vortices increases with system size. With our method, for system sizes up to N=250 and for the nearly uniform distribution of vortices typically found, the maximum number of inaccessible roots is one, and for that one we know that it is very near the south pole.

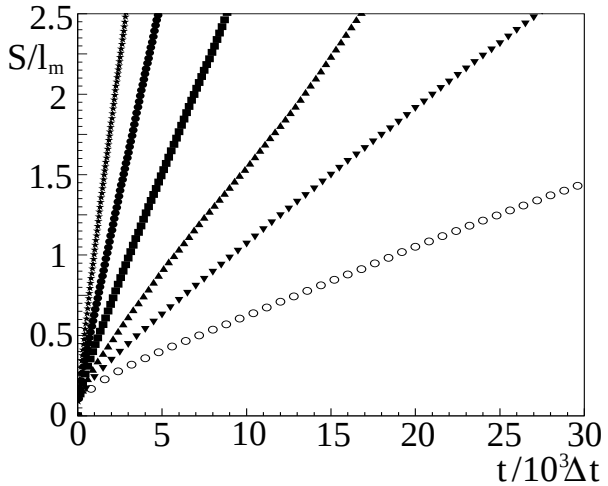

FIG. 6. $\langle (\mathbf{R}(t) - \mathbf{R}(0))^2 \rangle$ against t for $\alpha_T = -7$ (stars), $\alpha_T = -8$ (dots), $\alpha_T = -9$ (squares), $\alpha_T = -10$ (triangles pointing up), $\alpha_T = -11$ (triangles pointing down), $\alpha_T = -12$ (circles)

Once the roots are found, we have to identify the same vortex at different times in order to compute its self-diffusion. This was done by simply recording the vortex positions in short time intervals Δt and making a one-to-one mapping of the positions at t into the set at $t + \Delta t$ by pairing the vortices which are the smallest distance apart. Only very rarely these mappings were not one-to-one, but they could aways be made so by pairing one new position with its second or third nearest old position.

We have recorded the self-diffusion for a system of 200 vortices and effective temperatures α_T=-7,..,-12 for 13 (α_T=-7) to 22 (α_T=-12) times the density correlation relaxation time τ_D. A plot of S(t) as defined in Eq. (18) can be seen in Fig. 6. The dependence is linear except for very small times t. We have extracted D_s from fits to the linear regime according to Eq. (18). We are interested in how the diffusion time scale $\tau_{SD} \propto 1/D_s$ relates to the relaxation time scale of the density correlations τ_D. Fig. 7 shows both time scales plotted logarithmically against α_T. The data suggests the same linear exponential dependence $\tau \propto \exp(C|\alpha_T|)$ holds for both time scales. If we extract the gradient C from the linear fits in Fig. 7 for the data for D_s and for τ_D for the same system size, they agree within 7%. This agreement suggests that self-diffusion as well as relaxation processes in the system are determined by the same mechanism, with an activation energy that grows linearly with $-\alpha_T$.

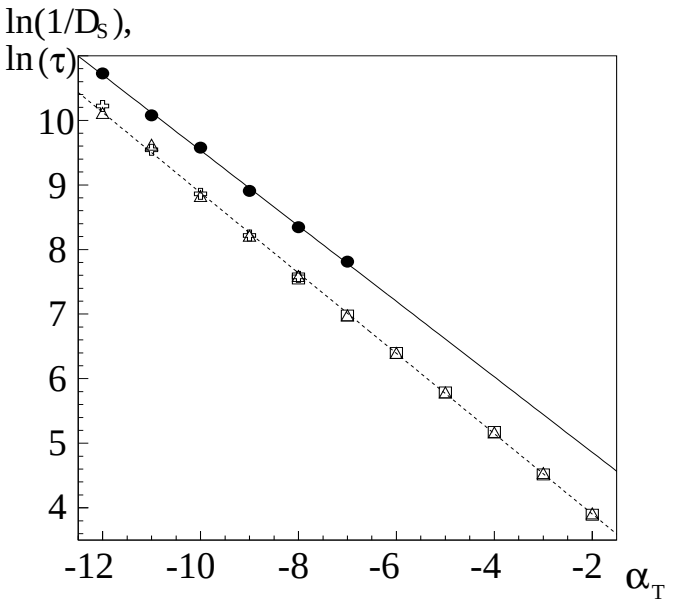

FIG. 7. Dominant time scales versus $-\alpha_T$ for D=0 (pure limit). Empty squares, triangles and crosses: Logarithm of the largest relaxation time scale for system sizes of N=72 ($2 \le -\alpha_T \le 8$), 200 ($2 \le -\alpha_T \le 12$), and 224 ($8 \le -\alpha_T \le 12$) respectively. The dotted line is a linear fit for N=200. Filled circles: Logarithm of the inverse self-diffusion coefficient for N=200 with linear fit (solid line)

VI. ACTIVATED DYNAMICS

We now put together our results regarding length and time scales in the thin film. Firstly, the length scale of translational order $\xi_D \propto \delta^{-1}$ has been measured [15] and calculated [7] in the pure limit from the structure factor. It increases as $\xi_D \propto -\alpha_T$ at low temperatures. We found that this is at least approximately true in a disordered system, a result in good agreement with analytical results [7]. Secondly, there is one dominant time scale τ which determines relaxation and self-diffusion times. It can be described as $\tau \propto \exp(-C\alpha_T)$. Again this behavior is not qualitatively changed by disorder. These two results together yield

$$\tau \propto \exp(F\,\xi_D/l_m). \tag{20}$$

Activated dynamics is said to occur when the time scale varies exponentially with some power of the correlation length. This kind of dynamics, which is found to be valid for example in spin glasses [30] is generally described by $\ln(\tau) \propto L^{\psi}$. Here L is the linear domain size, in our case given by ξ_D. The barrier-height exponent ψ describes how the activation energy of the dominant relaxation process, E_a, depends on the linear domain size. In our system ψ=1 and $E_a \propto k_B T \xi_D$. The proportionality constant F depends on the strength of disorder D. In Fig. 8 we have plotted $\ln(\tau)$ versus (δ^{-1}) for different disorder strengths. The poor quality of our data does only allow a quantitative description of $F(D)$. However, we can fit the data in the moderate to low temperature regime for weak disorder according to Eq. (20) as shown in the inset of Fig. 8. A clear decrease of the gradient of the linear fits (and hence F) with increasing disorder D is visible.

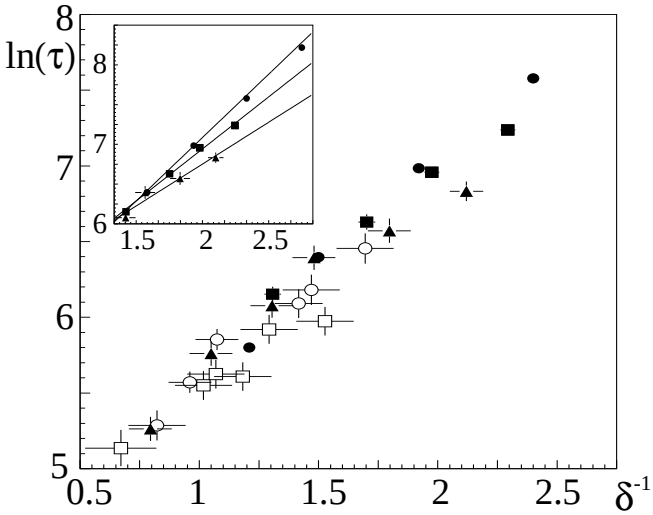

FIG. 8. The data from Figs. 5 and 2 plotted as $\ln\tau$ versus δ^{-1}. Filled circles, filled squares, triangles, empty circles, and empty squares correspond to D=0, 0.25, 1, 4, and 9 respectively. The inset shows the data for the temperature regime $-9 \le \alpha_T \le -6$ and weak disorder (D=0, 0.25, 1) with linear fits.

A. The relaxation mechanism

Fig. 9 shows snap shots of the vortex dynamics at $\alpha_T = -11$. The vortex motion is shown over half a self-diffusion time $\tau_{SD}(\alpha_T)$. After this time the average displacement of a vortex is l_m, which is $(\sqrt{3}/4\pi)^{1/2} \approx 0.37$ times the nearest neighbor distance in the triangular lattice ground state. The vortex positions are shown for 24 time steps Δt between initial and final position. To cut out small random moves and thus make the overall displacement of a vortex more clearly visible, the positions in the picture at time t are an average of the vortex positions at times $t - \Delta t$, t and $t + \Delta t$. The different grey shades of the vortex positions indicate their coordination number. The coordination numbers are not based on the time averaged, but on the real positions. The nearest-neighbor bonds at initial and final positions are also shown.

To identify pairs of nearest neighbors and calculate the coordination numbers we used a "greedy" triangulation algorithm. It uses the following definition of nearest neighbors in non-crystal context: Two vortices are nearest neighbors if their connection line does not cross with any other belonging to a pair a shorter distance apart. To apply this definition to a given configuration, the vortices are paired in all possible combinations and all pairs ordered according to distance. Then it is decided successively, starting from the pair with the shortest distance, if the vortices of a pair qualify as nearest neighbors, in which case they are connected with a bond. A pair is not connected with a nearest neighbor bond if its connection line crosses over one of the already existing nearest neighbor bonds. If this is not the case, the vortices in the pair are nearest neighbors and a bond is drawn.

We want to point out the main features about the vortex dynamics that can be learned from snap shots like the one in Fig. 9. At first sight they look quite confusing, no easy patterns being distinguishable even after the vortex paths have been smoothed out. The real relaxation mechanisms are not nicely isolated processes in an otherwise crystalline environment. We do for example not see "braids" as suggested in reference [15], which are formed by isolated motion of a ring of vortices. Where motion occurs, it does extend over a region of the plane. We also see that the vortices in the regions of motion change their coordination number very often. Topological defects such as dislocations, equivalent to a pair of one fivefold and one sevenfold coordinated vortex, occur in large numbers and their arrangements may be very transient, especially

at higher temperatures. The kind of relaxation process we see takes place in a more or less strongly correlated liquid and is not well described in terms of isolated topological defects in an elastic environment.

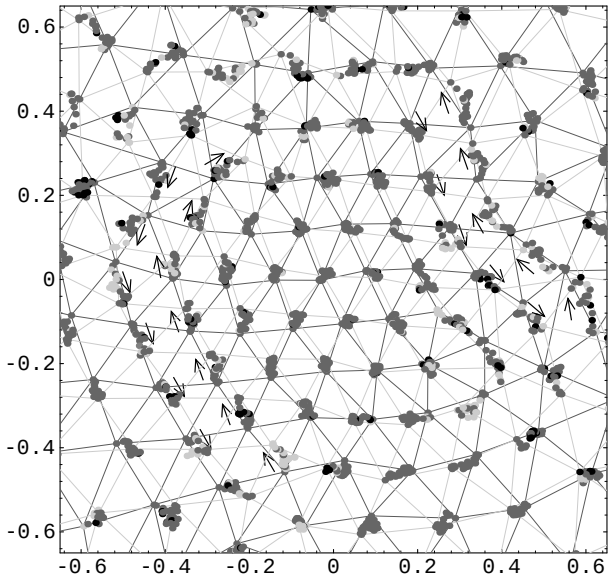

FIG. 9. Snap shots of the vortex motion in stereographic projection (r=0 is the north pole, r=1 is the equator) at $\alpha_T = -11$. The nearest-neighbor bonds are in darker grey for the starting points and in lighter grey for the end points. The vortex positions are shaded in lighter grey if their coordination number is $\leq$5, in medium grey if it is 6 and in black if it is $\geq$7. Arrows point out opposite parallel motion of vortex chains .

However, at a second look recurring themes in the vortex motion become visible. The kind of structure which is easiest to spot is a chain-like motion of vortices. The process underlying this chain motion can be identified as a tilt in the orientation of the nearest-neighbor grid in a strongly correlated region of the vortex liquid. In Fig. 9 such a tilt is easiest to spot as a small clockwise rotation about the mid point. However, a rotation of the underlying grid is not caused by a solid body rotation of all the vortices in the region. For a large correlated region, a solid body rotation would mean that vortices far from the center have to travel a long way, which does not happen. Instead each vortex moves in a way to reach a position in the new grid which is not too far from its initial position. In Fig. 9 this effect can be seen in the form of an opposite parallel motion of chains of vortices indicated with arrows.

We are confident that we see a genuine property of the 2D liquid and not a relaxation process favored by the fact that on the surface of a sphere there is a permanent presence of 12 5-coordinated centers (for detailed discussion refer to [15]). If these disclinations were crucial for the relaxation mechanism, one should expect the relaxation times to be larger in larger systems, where these defects are less concentrated. Fig. 7 however shows excellent agreement of τ_D for systems different in size by more than a factor 3.

B. Activation energy scaling

We observe that the typical length of moving chains increases with decreasing α_T. This is easy to understand because the range of hexatic order $\xi_D \propto -\alpha_T$ determines the size of a tilt region. This pattern of fewer, large events of motion at low temperature and smaller, uncorrelated events at higher temperature is confirmed by our self-diffusion measurements, where it can be deduced from the statistical error in the self-diffusion coefficient; if the simulation has been running for the same time in units of relaxation times, $t/\tau(\alpha_T)$=const., at different α_T, the vortices in the systems have diffused by the same amount but the error is clearly smaller at higher temperatures. The range of static correlations in the liquid determines the size of a tilt region and therefore the energy barrier height of the relaxation mechanism. To explain why the activation energy E_a depends linearly on ξ_D, we suggest the following scaling argument.

Consider a region of the vortex liquid with linear size ξ_D. We want to estimate the energy it costs to tilt the core of the region, while the edges relax, as can be seen in Fig.9, in order to keep best possible hexatic order with the static surroundings. Over a distance ξ_D hexatic correlations from the middle of the region to the edges are only just noticeable. Therefore the core of the region cannot rotate freely. The angles which allow some hexatic alignment with the surroundings are discrete in steps of $2\pi/N$, where N is the number of vortices on the edge on the region. The potential energies of the N different orientations with respect to the minimum energy orientation will have a probability distribution $P(E)$ with mean $\overline{E}$. A region of size ξ_D is typically in a low energy state just locked to a given orientation by its surroundings. The locking energy, which is the lowest potential difference E to one of the N other orientations, denoted $E_{\min}$, is of order k_BT. By rotating, the system will jump from an initial low energy state to higher ones. From there, the rotated region and its surroundings relax to a new low energy state, which is is the process responsible for destruction of correlations. The intermediate "barrier" state after the rotation is one of the N possible orientations, and its energy is a random energy from the distribution $P(E)$. We can write the typical activation energy as $E_a = \overline{E}$. From above we know that the typical lowest energy in a given sample $\overline{E_{\min}} \approx k_BT$. In order to find $\overline{E}$ we can apply the well-known result that the minimum value of E which occurs in a large random sample of size N is on average $\overline{E_{\min}} \propto \overline{E}/N$. This result is shown to be valid for any finite probability distribution

$P(E)$, $E \geq 0$ with mean $\overline{E}$ in Ref. [27]. We now know that $E_a = \overline{E} \propto N E_{\min} \approx N k_B T$. N is essentially the region's perimeter and therefore $N \propto \xi_D$, which yields $E_a \propto \xi_D \, k_B T$, the scaling behavior observed in our measurements.

VII. CONCLUSIONS

We have analyzed the equilibrium dynamics of a thin film superconductor in the vortex liquid phase. We have shown that there is one main relaxation time scale which appears in the decay of density correlations of the order parameter as well as in the self-diffusion of the vortices. This time scale shows a linear exponential dependence on α_T at all accessible temperatures. We have also described the effects of quenched random disorder on the density correlations and their decay. Disorder induces permanent correlations and reduces the range of the non-permanent correlations and their relaxation times. The density correlations in a disordered system look very similar to those in a system without disorder at a higher temperature. This is in good agreement with non-perturbative analytical results [7]. We find that both the pure and the disordered system have activated dynamics. The main time scale τ scales with the range of translational order ξ_D like $\tau \propto \exp(F \, \xi_D / l_m)$, where F depends on the strength of disorder. This indicates an activated relaxation process with an activation energy of the order $E_a \propto k_B T \; \xi_D / l_m$. We have identified this process as a tilt in the hexagonal orientation of the vortex liquid over a region of linear extent ξ_D. We have found no divergence of time scales or other features attributable to a phase transition at any finite temperature. Our work does not confirm the existence of a vortex lattice phase at finite temperature, nor do we see a vortex glass or Bragg glass phase in the disordered system.

Experimental results on time scales from ac transport measurement spectra in weakly disordered very films should provide information on the relaxation time scales found in our numerical work. Such experiments have been performed, see for example Refs. [18] and [19]. However, the samples in thin film experiments are are often two dimensional only in the sense that their characteristic bending length of vortices is larger than the sample thickness, but not thin enough to obey 2D LLL scaling. Therefore they do not compare directly to our results. Experiments similar to the ones from Refs. [18] and [19] but in thinner films would be directly related to our results. Experimental observation of self-diffusion would be far more difficult, if not impossible. Decoration experiments, which use snap shots of the vortex liquid, have made detailed studies of static properties possible (see e.g. [28] [29]). However, the analysis of the vortex dynamics with this technique remains difficult [28].

ACKNOWLEDGEMENTS

We would like to thank Tom Blum and Matthew Dodgson for useful interactions. AKK acknowledges financial support from a Manchester University Research Studentship and EPSRC.

[1] A. Fetter and P. Hohenberg, in *Superconductivity*, edited by R. Parks (Dekker, New York, 1969), Vol. 2.
[2] G. Eilenberger, Phys. Rev. **164**, 628 (1667).
[3] B. I. Halperin and D. R. Nelson, Phys. Rev. B **19**, 2457 (1979).
[4] S. Doniach and B. A. Hubermann, Phys. Rev. Lett. **42**, 1169 (1979).
[5] D. S. Fisher, Phys. Rev. B **22**, 1190 (1980).
[6] M. A. Moore, Phys. Rev. B **45**, 7336 (1992).
[7] J. Yeo and M. A. Moore, Phys. Rev. B **54**, 4218 (1996), Phys. Rev. Lett. **76**, 1142 (1996).
[8] A. I. Larkin, Zh. Eksp. Teo. Fiz. **58**, 1466 (1970).
[9] A. I. Larkin and Yu. N. Ovchinnikov, J. of Low Temp. Phys. **34**, 409 (1979).
[10] T. Giamarchi and P. Le Doussal, Phys. Rev. Lett. **72**, 1530 (1994); *ibid.* **74**, 606 (1995).
[11] J. Hu and A. H. MacDonald, Phys. Rev. Lett. **71**, 432 (1993); Phys. Rev. B **49**, 15263 (1994) .
[12] Y. Kato and N. Nagaosa, Phys. Rev. B **47**, 2932 (1992); **48**, 7383 (1993).
[13] J. A. O'Neill and M. A. Moore, Phys. Rev. B **48**, 374 (1993).
[14] H. H. Lee and M. A. Moore, Phys. Rev. B **49**, 9240 (1994).
[15] M. J. W. Dodgson and M. A. Moore, Phys. Rev. B **55**, 3816 (1997).
[16] P. Berghuis and B. H. Kes, Phys. Rev. B **47**, 226 (1993).
[17] A. V. Nikulov, D. Y. Remisov and V. A. Oboznov, Phys. Rev. Lett. **75**, 2586 (1995).
[18] A. Yazdani *et al.*, Phys. Rev. Lett. **70**, 505 (1993); Phys. Rev. B **50**, 16117 (1994).
[19] M. H. Theunissen, E. Van der Drift, and B. H. Kes, Phys. Rev. Lett. **77**, 159 (1996).
[20] M. A. Moore, Phys. Rev. B in press.
[21] R. Ikeda, J. Phys. Soc. Jpn. **64**, 1683 (1994).
[22] S. M. Roy and V. Singh, Phys. Rev. Lett. **51**, 2069 (1983).
[23] J. J. Binney *et al., The Theory of Critical Phenomena*, (Oxford Science Publications, Oxford 1992), chap. 4.
[24] R. Ettalaie and M. A. Moore, J. Phys. A : Math. Genn. **17**, 3505 (1984).
[25] A. K. Kienappel and M. A. Moore, in preparation.
[26] W. H. Press *et al., Numerical Recipes in C*, (Cambridge University Press, Cambridge 1992), chap. 9.5.
[27] A. J. Bray and M. A. Moore, in *Proceedings of the 1986 Heidelberg Colloquium on Glassy Dynamics*, edited by J.

L. v.Hemmen and I. Morgenstern, (Springer, Heidelberg, 1987)
[28] M. V. Marchevsky, PhD. thesis, University of Leiden, Netherlands (1997).
[29] P. Kim, Z. Yao, and C. M. Lieber, Phys. Rev. Lett. **77**, 5118 (1996).
[30] D. S. Fisher and D. A. Huse, Phys. Rev. B **38**, 373 (1988).